Analysis of the Carrier Suppressed Single Sideband Modulation for Long Distance Optical Communication Systems

Fadil Paloi, and *Shyqyri Haxha

Department of Electronic Engineering
Royal Holloway, University of London, Egham, Surrey, TW20 0EX, United Kingdom,
*Shyqyri.Haxha@rhul.ac.uk

Abstract: In this research paper, we report on a simulation study of the Radio over Fibre (RoF) Carrier Suppressed Single Sideband (CS-SSB) modulation scheme. This scheme is based on a Dual Parallel Dual Drive Mach-Zehnder modulator (DP-DDMZM), for a long-distance transmission. The proposed system consists of the combination of a carrier and a message signal at two parallel modulators, where the laser and link power is varied for the two different dispersion compensation techniques. We found that by suppressing the optical carrier and cancelling one sideband, we can limit the nonlinear effects that are caused by power fading and interference. We demonstrate that by varying the launched laser and link power up to optimised threshold levels, the signal to noise ratio (SNR) increases and the Q-Factor improves significantly. Our proposed RoF optic communication architecture can support an extended reach transmission of up to 200km without dispersion compensation. Moreover, for the bitrate of 10 Gbit/s and span length of 25 km, we achieved a span ratio of 520, alternatively viewed as the system link signal transmission distance of 13000 km. Therefore, this method is cost-effective and less complex.

Keywords: Single Sideband Modulation; Fibre optics communications; Carrier Suppression; Radio Over Fibre; Single Mode Fibre.

1. Introduction.

Radio-over-fibre (RoF) signal transmission has experienced tremendous growth and has had great interest for the research community in the last decades. This increased interest is due to the high capacity that the fibre optic system offers and the transparency of the system to the modulation and transmission. This transparency is beneficial for future system upgrades. Despite the significant advantages that RoF offers, there are still issues that the fibre optic system faces. These issues are consequence of the modulation, nonlinear effects, fibre chromatic dispersion, and other associated transmission losses [1]. It is known that losses can be improved by increasing the quality of the optical signal at the modulation [2]. However, for long distance transmission, dispersion is a major limiting factor that causes degradation of the signal transmission, and diminishes the data rate.

One of the key tasks when designing RoF systems is finding the method to modulate the signal into an optical carrier while achieving the least possible losses. Overall, there are three main factors limiting signal transmission at the fibre optic communication; nonlinear effects, attenuation, and dispersion. Many techniques have been proposed to compensate these losses. These techniques are divided in to; pre-distortion compensation at the transmitter, inline compensation at the channel, and post-spotted at the receiver [3, 4]. The transmission of the RF signal over the fibre optic link can be improved by the optical carrier suppression [4], given that the optical carrier takes most of the optical power and does not carry any information. Several methods have been utilised to generate linearized signal modulation by deploying two or more electro-optic modulators [5]. To improve the overall

system performance, several inline compensation techniques have been proposed, specifically Dispersion Compensation Fibre (DCF) [6] and Fibre Bragg Grating (FBG) [7]. FBG is one of the most used techniques due to its low insertion losses, low-cost, and most importantly, its compatibility within the existing optical communication structure configuration. In our transmission system, to observe the performance of the RoF, we have used a coherent detection with bias values from 1 (V) to 6 (V) as a function of output power. Based on Ref. [4], to reduce the RF power fading and interference between two bits, the minimum transmission point (mTP) is applied to both modulators at the push-pull configuration. This resulted in maximum optical carrier suppression and the complete cancelation of one of the sidebands. This occurred by increasing the gain of the useful signal on the optical sideband and improving the efficiency of the message signal transmission. Taking in to account system deteriorations due to the nonlinear effects at the channel link, we have investigated two compensation techniques for 10 Gbit/s and 40Gbit/s at three different stages of launched laser power and link power.

2. Methodology

We have developed a thorough analytical model and compared various modulation formats using CS-SSB optical modulation schemes. We have also deployed VPI simulation software packages [8] to implement the analytical model, and to scrutinise the proposed system performance. Initially, we studied a few action points, investigating the behaviour of the harmonics as a function of biased voltage in the CS-SSB configuration spectrum, as illustrated in Fig. 1a and Fig.1b. As demonstrated by these figures, the bias voltage significantly affects the system's performance, particularly impacting the harmonic distortion [9]. Both modulators are biased at various RF and DC switching voltages from $V\pi =1(V)$ up to 6 (V) as a function of output power, operating at mTP point for $V_{Bias} = V_\pi$, by changing $V_{bias1} = 1(V)$ up to 6(V) and $V_{bias2} = 0(V)$. The 90° phase shifter is applied to the input of the first child modulator and the output of the second child modulator, which makes the parent modulator biased at a quadrature point [10].

By increasing the bias voltages, the carrier for any input power is practically constant, as compared to the sidebands which are gradually decreasing. The existence of Second Order Harmonic (SOH) and Third Order Harmonics (TOH) depends on bias voltage. The higher the bias level, the smaller the harmonics and the higher the Dynamic Range (DR) [11].
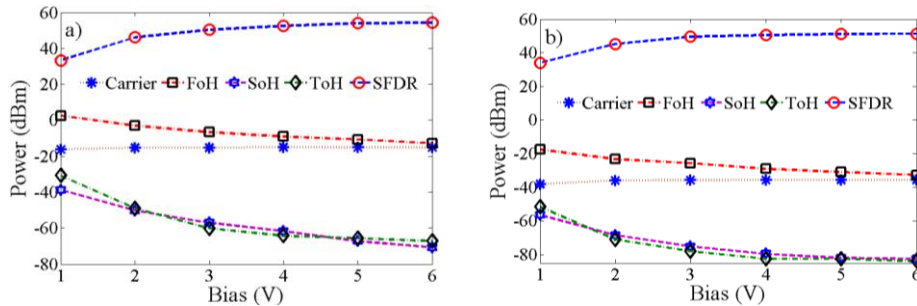

Fig.1. Behaviour of harmonics and the analysis on Dynamic Range (DR), variation of the bias as a function of the output power at the coherent detection; a). Optical output power, and b). Electrical output power.

By keeping the bias at 3 (V) in the transfer function, where the halfway switching voltage is $V\pi = 3$ (V), we managed to suppress the even order distortion, while leaving the third order as the dominant distortion product. The analytical calculations and simulation testing taken at the optical and RF side, are illustrated in Table1.

Optical and RF Spectrum Analysis at the Coherent Detection		
	Optical Spectrum	RF Spectrum
Carrier	J_0 = -15.18 dBm	J_0 = -35. 68 dBm
Fundamental	J_1 = -6.54 dBm	J_1 =-25.67 dBm
SOH	J_2= -60.14 dBm	J_2= -75.25 dBm
TOH	J_3= -57.02 dBm	J_3 = -78.11 dBm

SFDR	J_1-J_3= 50.48 dBm	J_1-J_2= 49.58dBm

Table 1. Optical and RF Spectrum Analysis at the Coherent Detection

The difference between the fundamental and highest harmonic (spur) gives us the spurious free dynamic range at the optical spectrum SFDR= f_1-f_3 = 50.48 dBm, and at the RF spectrum SFDR= f_1-f_2 = 49.58 dBm. The optical and RF spectrum, illustrated in Table 1, demonstrates the consistency between both sides of the transmission link.

3. Performance Parameters

To evaluate the performance of the proposed system, the DR is used as a key performance indicator, which is the difference between the fundamental and highest spur. In our proposed RoF system, the BER is specified as 10^{-9}, corresponding to the value of Q-Factor equal to 6. The relationship between Q-Factor and BER can be expressed as:

$$Q = \sqrt{2} \cdot erfc^{-1}(2 \cdot BER) \text{ or } Q = \frac{(\mu_1 - \mu_0)}{\sigma_1 + \sigma_0} \tag{1}$$

Where Q-Factor is defined as a ratio between the optical signal intensity of the higher and lower levels, and the standard deviation of the higher and lower levels in the eye diagram [12].

4. Proposed RoF Optical Configuration System

A. CS-SSB modulation scheme

The CS-SSB modulation scheme belongs to the transmission subsystem, and it consists of two similar DDMZMs driven by two equal electrical signals. The message signal (RF) was modulated with a carrier wave light through two parallel connected DDMZMs, embedded in to two arms of the parent MZM_3 structure. Initially, we used the system without any modulation format. To improve transmission performance, we employed a CS-SSB modulation scheme with an optimal sideband to spur ratio [1].

By accurate shifting between two DDMZMs, the CS-SSB modulation can be achieved where the suppressed carrier and upper or lower sidebands have been removed [13]. The CS-SSB schematic is illustrated in Fig.2, it consists of the Continues Wave Laser (CWL), operating at a frequency of 193.1 THz, with the optical power of 14dBm, which is split in to two paths, using a Y-branch coupler (3dB optical splitter) in to each DDMZM. The RF source signal with the input power of 10dBm, is electrically phase shifted by a 90^0-hybrid coupler, both are divided in to two equals sub-MZMs, with first child MZM_1 defined as *cosine*, and second child MZM_2 defined as *sine*-wave signal. Subsequently, two RF messages are divided in two equivalent arms, the upper and lower RF for each DD-MZM [14].
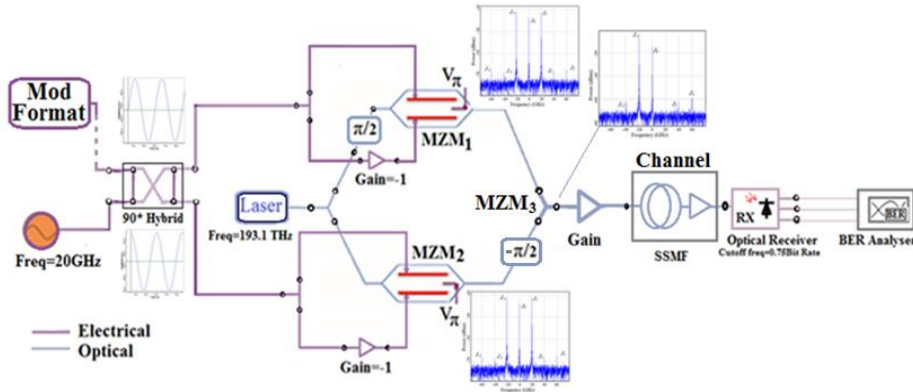

Fig. 2. Schematic diagram of the proposed RoF system based on the CS-SSB modulation for long distance signal transmission

In our model the optical carrier light at the input of DDMZM can be expressed as [15]:

$$E_{in}(t) = \sqrt{2kP_0} \cdot e^{j\omega_0 t} \cong \sqrt{2}E_0 \cdot e^{j\omega_0 t} \tag{2}$$

Where, E_{out} is laser output optical field, P_0 is the average laser power, k is constant related to the average power and the optical field. E_0 is known as the optical carrier amplitude at the angular frequency ω_0 with initial phase φ_0. The optical losses, including insertion waveguide propagation losses, splitting and coupling losses are assumed to be 6 (dB). Both modulators are assumed to be identical, with the same driving RF signal voltages [15]. The device design parameters utilized in our proposed structure configuration are based on the structure parameters published in Ref. [16 and 17]. In our proposed structure modulators have encoded 10Gbit/s data at the pseudo random binary sequence, compare to 2.5 Gbit/s encoded by the Ref. [17]. In Fig. 3, we illustrate the simulation configuration of the first child DD-MZM for the 20GHz single tone signal.
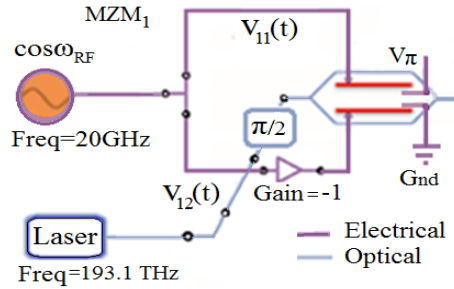

Fig. 3. Schematic configuration of DD-MZM1, generating Carrier Suppressed Sideband signal.

The carrier signal is instantly mixed at the DD-MZM with the modulating signal applied to the upper and lower electrodes [4]. The voltages required to shift the phase of the light by one half a wavelength, compared to the other $V_\pi=3$ (V), are known as RF and DC (Bias) switching voltages ($V_{\pi RF}$ and $V_{\pi DC}$) [17, and 18]. V_{bias1} and V_{bias2} are the bias voltages applied to both arms of the first child modulator (MZM$_1$). The MZM$_1$ illustrated in Fig.3, is arranged at the push pull configuration mode, where two arms (two drives with data and inverted data) are used to generate intensity modulation. The RF modulating electrical voltages, $V_{11}(t)$ and $V_{12}(t)$ are expressed as cosines, and inverted cosine, Eq. (3, 8). The amplitude V_{11} of the RF drive signal is applied to upper electrode of the first child modulator. In addition, the optical phase difference $\Phi_{11}(t)$ exists in the upper arm through the electro-optic effect, Eq. (4)

$$V_{11}(t) = V_{11} \cos \omega_{RF} t + V_\pi \tag{3}$$

$$\Phi_{11}(t) = \pi \frac{V_{11}(t)}{V_\pi} = \pi \frac{V_{11}}{V_\pi} \cos \omega_{RF} t + \pi \frac{V_{\pi dc}}{V_\pi} \tag{4}$$

The RF signal using Eq. (3) is applied on the upper arms of the MZM1, whereas the optical field in the upper arm can be expressed as:

$$E_{Upper1}(t) = \frac{E_0}{\sqrt{2}} e^{j\omega_0 t} \left\{ e^{j\pi \frac{V_{11}}{V_\pi} \cos \omega_{RF} t} \cdot e^{j\pi \frac{V_{\pi dc}}{V_\pi}} \right\} =$$

$$\frac{E_0}{\sqrt{2}} e^{j\omega_0 t} \left\{ e^{jm \cdot \cos \omega_{RF} t} + e^{j\pi} \right\} = \frac{E_0}{\sqrt{2}} e^{j\omega_0 t} \left\{ -e^{jm \cdot \cos \omega_{RF} t} \right\} \tag{5}$$

4

To achieve the carrier suppressed signal, the bias voltage of MZM$_1$ is set at the mTP, with $V_{Bias} = V_{bias1} - V_{bias2} = V_\pi$, at the specific selected value of $V_{bias1} = 3[V]$ and $V_{bias2} = 0[V]$.

Where $m = \pi \dfrac{V_{11}}{V_\pi}$, is modulation index, V_{11} is peak to peak or RMS voltage calculated after 3 dB coupler.

$$E_{Upper1}(t) = \frac{E_0}{\sqrt{2}}(\cos\omega_0 t + j\sin\omega_0 t) \cdot$$
$$\{-[\cos(m\sin\omega_{RF}t) + j\sin(m\sin\omega_{RF}t)]\} \tag{6}$$

Eq. (6) can be solved by using the Bessel function identities. After Jacoby-Anger expansion, the output electric field at the upper arm of the MZM$_1$ can be written as follows.

$$E_{Upper1}(t) = \frac{E_0}{\sqrt{2}}(\cos\omega_0 t + j\sin\omega_0 t) \cdot$$
$$\left\{ \begin{array}{l} -J_0(m) + 2J_2(m)\cos 2\omega_{RF}t - \\ j2J_1(m)\cos\omega_{RF}t + j2J_3(m)\cos 3\omega_{RF}t \end{array} \right\}$$

$$= \frac{E_0}{\sqrt{2}} \left\{ \begin{array}{l} -J_0(m)\cos\omega_0 t \\ +J_2(m)\cos(\omega_0 t + 2\omega_{RF}t) + J_{-2}\cos(\omega_0 t - 2\omega_{RF}t) \\ +J_1(m)\sin(\omega_0 t + \omega_{RF}t) + J_{-1}(m)\sin(\omega_0 t - \omega_{RF}t) \\ -J_3(m)\sin(\omega_0 t + 3\omega_{RF}t) - J_{-3}(m)\sin(\omega_0 t - 3\omega_{RF}t) \end{array} \right\} \tag{7}$$

From the Eq. (7), in Fig. 4a, we have drawn the frequency vector diagram for Bessel function plans of MZM$_1$ upper branch. Due to the small coefficients, we have neglected the Bessel terms of a higher order than 3.

The amplitude V_{12} of the RF drive signal is applied to lower electrode of the first child modulator. Furthermore, the optical phase difference $\Phi_{12}(t)$ exists in the upper arm through the electro-optic effect, Eq. (9)

$$V_{12}(t) = V_{12}\cos(\omega_{RF}t + \pi) = -V_{12}\cos\omega_{RF}t \tag{8}$$

$$\Phi_{12}(t) = \pi\frac{V_{12}(t)}{V_\pi} = -\pi\frac{V_{12}}{V_\pi}\cos\omega_{RF}t \tag{9}$$

Based on the chirp modelling, when the modulator operates at push-pull mode, π is added to make the lower branch negative ($V_{21}(t) = -V_{22}(t)$) where the chirp is at its lowest value or it can be considered as the cancelled value [19].

$$E_{lower1}(t) = \frac{\sqrt{2}E_0}{2}e^{j\omega_0 t}\{e^{j\Phi_{12}(t)}\} = \frac{E_0}{\sqrt{2}}e^{j\omega_0 t}\left\{e^{-j\pi\frac{V_{12}}{V_\pi}\cos\omega_{RF}t}\right\} \tag{10}$$

$$= \frac{E_0}{\sqrt{2}}(\cos\omega_0 t + j\sin\omega_0 t)\left\{ \begin{array}{l} \cos(m\cos\omega_{RF}t) \\ -j\sin(m\cos\omega_{RF}t)] \end{array} \right\} \tag{11}$$

Also, Eq. (11) can be solved by using the Bessel function identities, after Jacoby-Anger expansion, the output optic field for the lower arm of MZM$_1$ can be written as [20].

$$E_{lower1}(t) = \frac{E_0}{\sqrt{2}}(\cos\omega_0 t + j\sin\omega_0 t) \cdot$$

$$\begin{Bmatrix} J_0(m) - 2J_2(m)\cos 2\omega_{RF}t \\ -j2J_1(m)\cos\omega_{RF}t + j2J_3(m)\cos 3\omega_{RF}t \end{Bmatrix} =$$

$$= \frac{E_0}{\sqrt{2}}\begin{Bmatrix} J_0(m)\cos\omega_0 t \\ -J_2(m)\cos(\omega_{RF}t + 2\omega_{RF}t) - J_{-2}(m)\cos(\omega_{RF}t - 2\omega_{RF}t) \\ +J_1(m)\sin(\omega_0 t + \omega_{RF}t) + J_{-1}(m)\sin(\omega_0 t - \omega_{RF}t) \\ -J_3(m)\sin(\omega_0 t + 3\omega_{RF}t) - J_{-3}(m)\sin(\omega_0 t - 3\omega_{RF}t) \end{Bmatrix} \quad (12)$$

Based on Eq. (12), in Fig. 4b we have drawn the frequency vector diagram for Bessel function plans for the lower branch of MZM$_1$ [19].
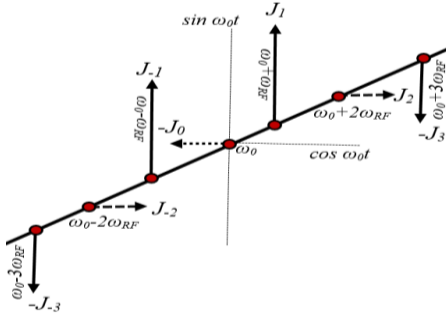
Fig.4a. Principle of CS-SSB modulation, showing frequency diagram for Bessel function outlines of upper branch MZM$_2$.
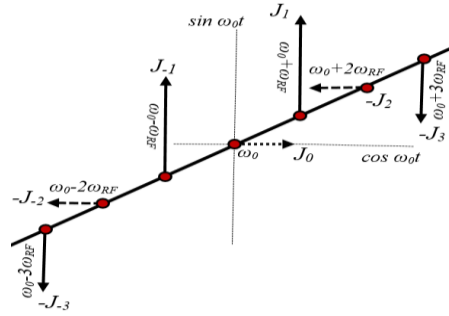
Fig.4b. Principle of CS-SSB modulation, showing frequency diagram for Bessel function outlines of lower branch MZM$_2$.

The optical power carried by the laser, reaches the input junction of the DD-MZM$_1$ with the transmission coefficient of $r_1 = r_2 = 1/2$, which is 50/50 ideal power splitting ratio or $r_1 = 1 - r_2$, where no phase modulation term exists [19].

$$E_{MZM1} = E_{Upper1} + E_{lower1} = E_0 e^{j\omega_0 t}\left\{\sqrt{r_1 r_2}e^{j\Phi_{11}(t)} + \sqrt{(1-r_1)(1-r_2)}e^{j\Phi_{12}(t)}\right\} \quad (13)$$

The MZM$_1$ output electric field is given by:

$$E_{MZM1} = \sqrt{2}E_0\begin{Bmatrix} 2J_1(m)\sin\omega_0 t \cdot \cos\omega_{RF}t \\ -2J_3(m)\sin\omega_0 t \cos 3\omega_{RF}t \\ +j[-2J_1(m)\cos\omega_0 t \cos\omega_{RF}t \\ +2J_3(m)\cos\omega_0 t \cos 3\omega_{RF}t] \end{Bmatrix} \quad (14)$$

$$E_{MZM1} = \sqrt{2}E_0\begin{Bmatrix} J_1(m)\sin(\omega_0 t + \omega_{RF}t) + J_{-1}(m)\sin(\omega_0 t - \omega_{RF}t) \\ -J_3(m)\sin(\omega_0 t + 3\omega_{RF}t) - J_{-3}(m)\sin(\omega_0 t - 3\omega_{RF}t) \end{Bmatrix} \quad (15)$$

Next, by combining the vector diagrams of two parallel branches of the first child MZM$_1$, Eq. (15), we can observe the maximum carrier suppression and even order harmonic cancellation, as illustrated in Fig. 5a.
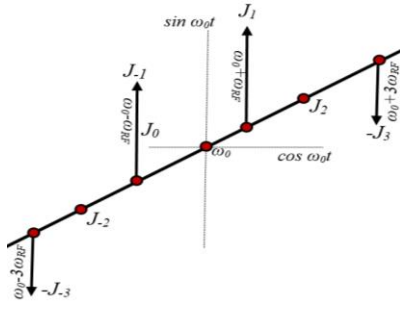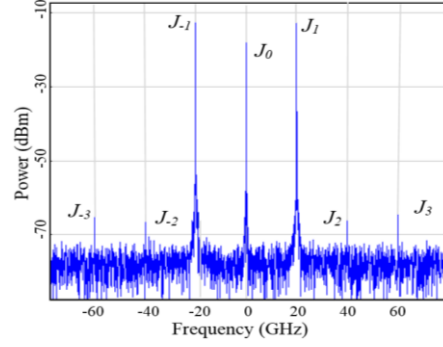
Fig. 5a: Propagated vector signal for the first child MZM$_1$

Fig. 5b: Optical spectrum of a CS- SSB generation for the first child MZM$_1$.

Furthermore, to achieve carrier suppressed modulation out of the second child modulator, the phase of the lower or upper arm of the MZM$_2$ must be configured at the push-pull configuration mode, 180^0 shifted compare to the other branch and biased at mTP. The schematic configuration of DD MZM$_2$ is illustrated in Fig. 6.
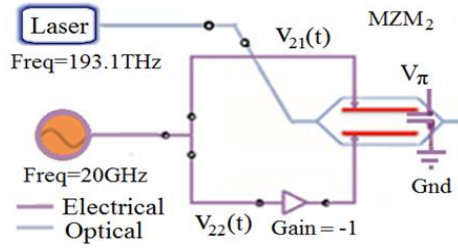

Fig.6. Schematic configuration of the second child DD-MZM

The RF modulating electrical signal is 3dB coupled in to two equal branches $V_{21}(t)$ and $V_{22}(t)$, defined as sine-wave and inverse sine-wave signal. The V_{21} and V_{22} are the signals amplitudes of the upper and lower arm of the second child modulator. The ω_{RF} is the angular frequency of the RF signal. The modulated electrical signal at the upper branch of the second child modulator, illustrated in Fig.6, can be expressed as:

$$V_{21}(t) = V_{21} \cos(\omega_{RF} t + \frac{\pi}{2}) + V_\pi = -V_{21} \sin \omega_{RF} t + V_\pi \qquad (16)$$

$$\Phi_{21}(t) = \pi \frac{V_{21}(t)}{V_\pi} = -\pi \frac{V_{21}}{V_\pi} \sin \omega_{RF} t + \pi \qquad (17)$$

In Eq. (17), we have expressed the optical phase difference $\Phi_{21}(t)$ which exists in the upper arms of the MZM$_2$ through the electro-optic effect, operating at the RF angular frequency ω_{RF}.

The output electric field at the upper arm of the MZM$_2$ can be written as:

$$E_{Upper2}(t) = \frac{\sqrt{2}E_0}{2} e^{j(\omega_0 t)} \left\{ e^{-j\pi \frac{V_{11}}{V_\pi} \sin \omega_{RF} t} + e^{j\pi} \right\}$$

$$E_{Upper2}(t) = \frac{E_0}{\sqrt{2}} (\cos \omega_0 t + j \sin \omega_0 t) \{-[\cos(m \cos \omega_{RF} t) - j \sin(m \cos \omega_{RF} t)]\} \qquad (18)$$

Eq. (18) can be solved by using the Bessel function identities. After Jacoby-Anger expansion [20], the output optic field for the upper branch of MZM$_2$ is.

$$E_{Upper2}(t) = \frac{E_0}{\sqrt{2}}(\cos\omega_0 t + j\sin\omega_0 t) \cdot \left\{ \begin{array}{l} -J_0(m) - 2J_2(m)\cos 2\omega_{RF}t \\ + j2J_1(m)\cos\omega_{RF}t + j2J_3(m)\cos 3\omega_{RF}t \end{array} \right\}$$

$$= \frac{E_0}{\sqrt{2}} \left\{ \begin{array}{l} -J_0(m)\cos\omega_0 t \\ -J_2(m)\cos(\omega_{RF}t + 2\omega_{RF}t) - J_{-2}(m)\cos(\omega_{RF}t - 2\omega_{RF}t) \\ -J_1(m)\sin(\omega_0 t + \omega_{RF}t) - J_{-1}(m)\sin(\omega_0 t - \omega_{RF}t) \\ -J_3(m)\sin(\omega_0 t + 3\omega_{RF}t) - J_{-3}(m)\sin(\omega_0 t - 3\omega_{RF}t) \end{array} \right\} \quad (19)$$

Based on Eq. (19), in Fig. 7a we have drawn the frequency vector diagram for Bessel function outlines of upper branch of MZM$_2$.

Based on the Push-Pull configuration, π is added to make the lower branch inverse compare to the upper branch. The optical phase difference $\Phi_{22}(t)$, existing in the lower arms of the second child MZM$_2$ through the electro-optic effect, operating at the angular frequency ω_{RF} is expressed in Eq. (21). The modulated electrical signal at the lower branch of the second child DD-MZM$_2$, illustrated in Fig.6, can be expressed as:

$$V_{22}(t) = V_{22}\cos(\omega_{RF}t + \frac{\pi}{2} + \pi) = V_{22}\sin\omega_{RF}t \quad (20)$$

$$\Phi_{22}(t) = \pi\frac{V_{22}(t)}{V_\pi} = \pi\frac{V_{22}}{V_\pi}\sin\omega_{RF}t \quad (21)$$

$$E_{Lower2}(t) = \frac{\sqrt{2}E_0}{2}e^{j(\omega_0 t)}\left\{ e^{j\Phi_{22}(t)} \right\} \quad (22)$$

$$E_{Lower2}(t) = \frac{E_0}{\sqrt{2}}(\cos\omega_0 t + j\sin\omega_0 t) \cdot$$
$$\{[\cos(m\sin\omega_{RF}t) + j\sin(m\sin\omega_{RF}t)]\} \quad (23)$$

From the Eq. (23), by using the Bessel function identities, and after Jacoby-Anger expansion [20], the outcome optic field for the lower branch of the second child MZM$_2$ is:

$$E_{Lower2}(t) = \frac{E_0}{\sqrt{2}}(\cos\omega_0 t + j\sin\omega_0 t) \cdot$$
$$\left\{ \begin{array}{l} J_0(m) + 2J_2(m)\cos 2\omega_{RF}t + \\ j2J_1(m)\cos\omega_{RF}t + j2J_3(m)\cos 3\omega_{RF}t \end{array} \right\}$$

$$\frac{E_0}{\sqrt{2}} \left\{ \begin{array}{l} J_0(m)\cos\omega_0 t + J_2(m)\cos(\omega_0 t + 2\omega_{RF}t) + J_{-2}(m)\cos(\omega_0 t - 2\omega_{RF}t) \\ -J_1(m)\sin(\omega_0 t + \omega_{RF}t) - J_1(m)\sin(\omega_0 t - \omega_{RF}t) \\ -J_3(m)\sin(\omega_0 t + 3\omega_{RF}t) - J_{-3}(m)\sin(\omega_0 t - 3\omega_{RF}t) \end{array} \right\} \quad (24)$$

Using Eq. (24), in Fig. 7b we have illustrated the frequency vector diagram for Bessel function of the lower branch MZM$_2$.
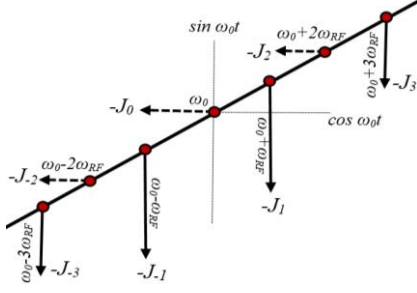
Fig.7a. Principle of CS-SSB modulation, showing frequency diagram for Bessel function outlines of upper branch MZM_2.
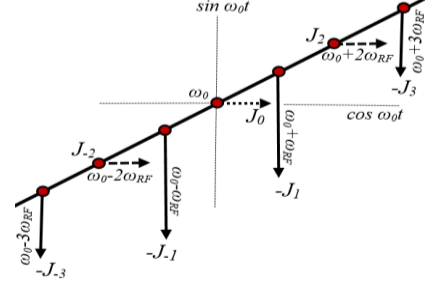

Fig.7b. Principle of CS-SSB modulation, showing frequency diagram for Bessel function outlines of lower branch MZM_2.

$$E_{MZM2} = E_{Upper2} + E_{lower2} = E_0 e^{j(\omega_0 t)} \left\{ \sqrt{r_1 r_2} e^{j\Phi_{21}(t)} + \sqrt{(1-r_1)(1-r_2)} e^{j\Phi_{22}(t)} \right\}$$

$$E_{MZM2} = \sqrt{2} E_0 \left\{ \begin{array}{l} -2J_1(m) \sin \omega_0 t \cdot \cos \omega_{RF} t \\ -2J_3(m) \sin \omega_0 t \cos 3\omega_{RF} t \end{array} \right\} \tag{25}$$

$$E_{MZM2} = \sqrt{2} E_0 \left\{ \begin{array}{l} -J_1(m) \sin(\omega_0 t + \omega_{RF} t) - J_{-1}(m) \sin(\omega_0 t - \omega_{RF} t) \\ -J_3(m) \sin(\omega_0 t + 3\omega_{RF} t) - J_{-3}(m) \sin(\omega_0 t - 3\omega_{RF} t) \end{array} \right\} \tag{26}$$

By combining the vector diagrams of two parallel branches of the second modulator (MZM_2), as shown in Fig. 8 we can observe maximum carrier suppression and even order harmonic cancellation, which results from the sidebands calculations achieved in Eq. (26) [16].
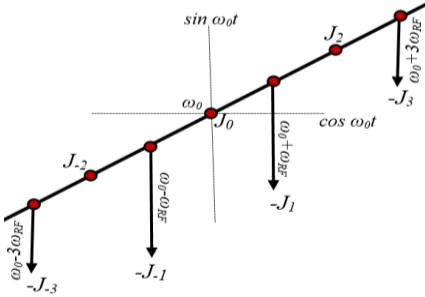

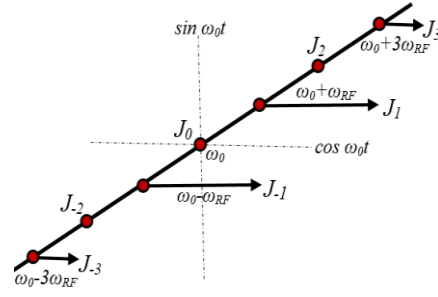Fig. 8a. Propagated signal based on the Bessel function profiles of $-Jn$ and Jn for the second MZM_2

Fig. 8b. Propagated signal based on the Bessel function profiles of $-Jn$ and Jn, after 90^0 shifting at the MZM_2

The output of the second child modulator (MZM_2) should be shifted by $-\pi/2$ to achieve CS-SSB signal at the output of the DP-DDMZM, as illustrated in Fig. 8b [18, 20]. The propagated output electric signal at the MZM_2 for in and out phase is given by Eq. 27. Each frequency diagram shows Bessel function profile from J_{-n} to $J_{n,}$ as illustrated in Fig. 8b.

$$E_{MZM2} = \sqrt{2} E_0 \left\{ \begin{array}{l} J_1(m) \cos(\omega_0 t + \omega_{RF} t) + J_{-1}(m) \cos(\omega_0 t - \omega_{RF} t) \\ + J_3(m) \cos(\omega_0 t + 3\omega_{RF} t) + J_{-3}(m) \cos(\omega_0 t - 3\omega_{RF} t) \end{array} \right\} \tag{27}$$
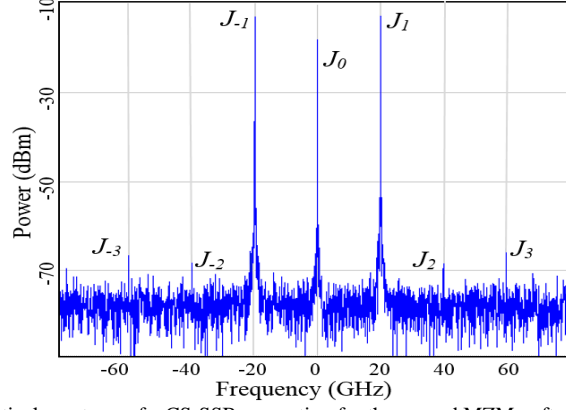
Fig. 9. Optical spectrum of a CS-SSB generation for the second MZM$_2$, after 90^{0}shifting.

The next step is to combine these two parallel DD-MZMs, where after 3 dB coupler the output optical field is:

$$E_{out}(t) = \frac{\sqrt{2}}{2}[E_{MZM1}(t) + E_{MZM2}(t)] = $$

$$= \sqrt{2}E_0 \begin{Bmatrix} 2J_1(m)\cos\omega_0 t \cdot \cos\omega_{RF}t - 2J_3(m)\sin\omega_0 t \cos 3\omega_{RF}t \\ + j[2J_1(m)\sin\omega_0 t \cos\omega_{RF}t + 2J_3(m)\cos\omega_0 t \cos 3\omega_{RF}t] \end{Bmatrix}$$

(28)

When the amplitude of the electric driving signal "V$_{p-p}$" is equal to switching voltage "V$_\pi$", then maximum modulation index can be achieved at $\pi/2$, cancelling even order harmonics, while maintaining the CS-SSB condition in Eq. (28) where:

$$E_{out}(t) = \sqrt{2}E_0 \{ + J_{-1}(m)\cos(\omega_0 t - \omega_{RF}t) - J_3(m)\sin(\omega_0 t + 3\omega_{RF}t) \}$$

(29)

Using on the Bessel function profiles and based on equation (29), in-phase modes such as J_{-1} and $-J_3$ are the output optical signals propagating through the Y junction. As can be seen from Eq. (29), and as illustrated in Fig. 10, the achieved optical spectrum of the signal generation with carrier and sideband suppression consists of the first and third sidebands, where J_{-1} and $-J_3$ represent the first and third order Bessel functions. Meanwhile, the zero order J_0 of the Bessel function is suppressed, the power level of other frequency components has increased. By applying peak to peak RF driving voltage to each modulator, or VRMS to each port, we have achieved the highest SFDR and maximum sideband power J_{-1}. Negative first order component J_{-1} shows the maximum optical power at the driving voltage of 3 (V). This is illustrated at both the Spectrum Analysers, shown in Fig. 11(a and b), and the analytical calculation designed by the vector diagram illustrated in Fig. 10.
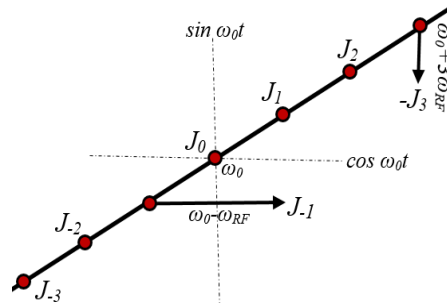

Fig. 10. Propagated signal based on the Bessel function profiles of J_{-1} and $-J_3$ for the parent MZM.

Based on equation (28), out-phase modes such as J_1 and $-J_{-3}$ are radiated optical signal.

10

5. Performance Analysis

A. Dynamic Range(DR)

The SFDR is one of the most crucial factors when planning the system of photonic link. The DR can be maximised if the noise floor level equals the distortion level. To observe the performance of the system, first we used coherent detection. The results at the output of the modulator must be comparable to results at the receiver side [9, 10]. Third order intermodulation distortion (IMD3) is very close to the spectrum of the signal. For the signal transmission, IMD3 is the most obstructive factor of the SFDR. Thus, the main aim is to suppress IMD3 as much as possible. Because of the minimum transmission point applied to both modulators, we have achieved optical carrier suppression, which increases the gain and effectiveness of message signal transmission, planed Fig. 10, by using Eq.29.

The optical spectrum illustrated in Fig. 11a demonstrates the suppression of harmonics, and the achieved SFDR is 50.48 [dBm]. The simulated electrical spectrum consists of the fixed 20 GHz signal frequency and the spurious of 40 GHz signal frequency.
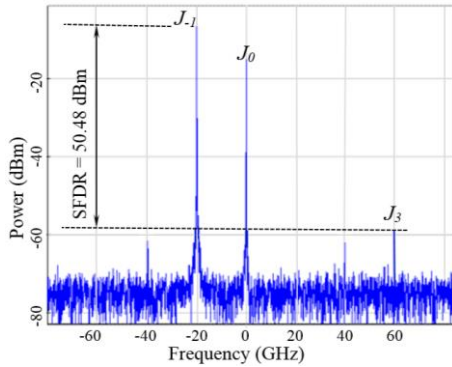

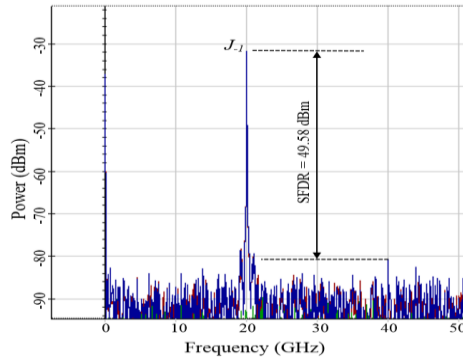Fig. 11. a) Optical spectrum of a CS-SSB generation at the output of Parent MZM

Fig. 11. b) Electrical spectrum of a CS- SSB generation at the RF site, after PIN photodiode

The spurious suppression ratio SFDR=49.58dBm is the difference between the signal and spur power after the link length of 25km calculated at the RF site as illustrated in Fig. 11.b.

The non-ideal factors which contribute to the performance of the system (SFDR) are: non-equal amplitudes applied to each electrode of the DP-DDMZM, switching voltages of each modulator, and extinction ratio which cannot be the same for both modulators [21, 22]. The SFDR performance and the suppression of the IMD3 is calculated by varying the RF input power [23]. The achieved power as a function of the input power for the fundamental, IMD3 and IMD2, for the proposed modulation scheme is illustrated in Fig. 12.
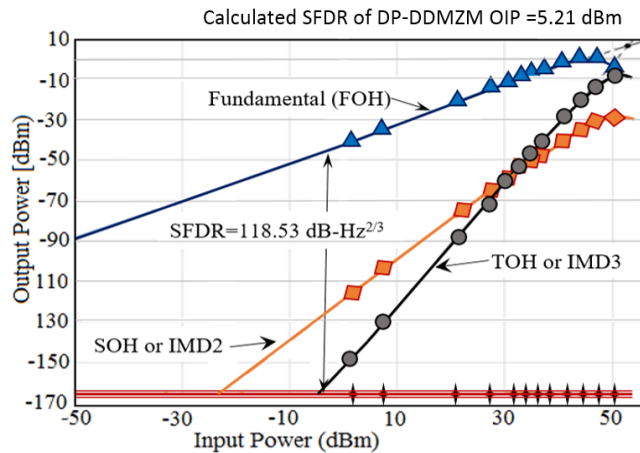

Fig. 12. Calculated SFDR at the DP-DDMZM, showing output power as a function of input power.

Based on our analysis and simulation results, the noise floor is dominated by the shot noise and thermal noise, value of 163.977dBm/Hz. With the stabilised RF input power and adequate bias voltage, the system performance of the proposed DP-DDMZM scheme has improved significantly, resulting in an SFDR of 118.53 dB/Hz$^{2/3}$ as illustrated in the Fig. 15. The output Third-Order Intermodulation Intercept (OIP3) is around 5.21dBm. Harmonics higher than SOH have been suppressed in the SC-SSB spectrum for the switching bias and RF voltages higher than 6 (V).

B. Comparison of two Compensation Techniques

Distortion caused due to the Chromatic Dispersion (CD) is evident, it originates from the mixing term of the power employed in the modulator [3, 23, 24]. When the CS-SSB signal propagates through the SSMF, the phase of each optical sideband relative to the optical carrier will change by chromatic dispersion. The propagation constant of the dispersion fibre expanded in Taylor series around carrier is:

$$\beta(\omega) = n(\omega)\frac{\omega}{c} = \beta_0 + \beta_1(\omega - \omega_c) + \frac{1}{2}\beta_2(\omega - \omega_c)^2 + .. \tag{30}$$

For the carrier tone at the central frequency $\omega = \omega_c \pm n\omega_{RF}$ [19].

$$\beta(\omega_c - n\omega_{RF}) \cong \beta_0 + n\beta_1(\omega_c)\omega_{RF} + \frac{1}{2}n^2\beta_2(\omega_c)\omega_{RF}^2 \tag{31}$$

β_0 is constant related to phase velocity of optical carrier, β_1 determines the group velocity which is related to group delay.

$$\beta_2(\omega_C) = -\frac{c}{2\pi f^2} \cdot D(\omega_C)$$

β_2 is derivation of the group velocity, related to the chromatic dispersion parameter D =16ps/nm/km, light speed in vacuum c, and optical carrier frequency fc.

The electric field after signal transmission over dispersive SSMF at the length distance z can be expressed:

$$E_{out}(t) = \sqrt{2}E_0 \cdot \{J_{-1}(m)\cos[(\omega_0 t - \omega_{RF}t) - \beta_0 z + \beta_1\omega_{RF}z - \frac{1}{2}\beta_2\omega_{RF}^2 z]$$
$$- J_3(m)\sin[(\omega_0 t + 3\omega_{RF}t) - \beta_0 z + 3\beta_1\omega_{RF}z - \frac{9}{2}\beta_2\omega_{RF}^2 z]\} \tag{33}$$

After photodetection, the photocurrent can be expressed as:

$$i(t) = R \cdot |E_{out}(t)|^2 = E_{out}(t) \cdot E^*_{out}(t)$$

Where R=0.8, is photodiodes responsivity.

We have seen that, by varying launched laser and link power up to a certain level, signal to noise ratio (SNR) will increase and Q-Factor will improve. However, based on our simulation model, very high RF power will degrade Q-Factor and will produce a higher level of nonlinearities. Thus, there are limits between RF power and lower level of nonlinearities.

The transmission performance of the system link is expressed in terms of the BER of 10^{-9}, demonstrated at DP-DDMZM for various transmission distance and bitrate, evaluated on the base of the Q-Factor, using Eq. (1).

The threshold of 6 is used as the Q-Factor value to check for the accessible distance and number of loops or splits that the system can manage.

At this stage, we have added to the system modulation format. We have implemented our proposed scheme with two different compensation techniques, the linear chirped FBG and conventional DCF carried out in our previous study Ref. [6]. The dispersion compensation maps used for both compensation techniques in the system link are pre, inline symmetrical, and post-compensation. To achieve the target performance for each modulation format we relied on our analytical and simulation results. Taking in to account a system weakened by the nonlinear effects at the channel link, we have investigated the system for 10 Gbit/s and 40Gbit/s at three different launched laser and link powers. The system link is based on the CS-SSB modulation, using standard single mode fibre (SSMF), setting attenuation to 0.2dB/km and dispersion to 16ps/nm/km. Dispersion for DCF has been setup to -80ps/nm/km with attenuation of 0.5dB/km. While using these settings, based on the DCF carried out in our previous study Ref. [6], the maximum signal transmission of up to 2400 km for the span length of 50km can be achieved, as illustrated in Fig.13.
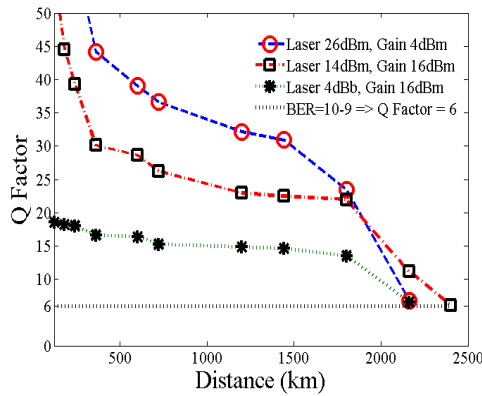

Fig. 13. Q-Factor versus various distance, using DCF, 50km SMF span length, at 10Gbit/s for various launched laser and link power.
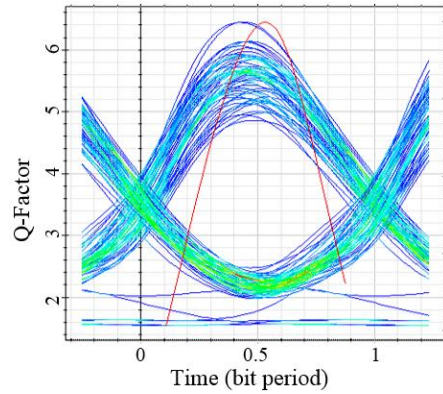
Fig.14. The eye diagram and Q-Factor of 6, consistent with BER of 10^{-9} for the length of 200(km) without any DCF.

To evaluate the transmission performance for the CS-SSB signal, based on Ref. [6, 17, 25], an analysis was performed at three different transmission powers, for the various span lengths.

- *At the laser power of 26dBm and gain of 4dB.*

By using the proposed CS-SSB modulation with the linear FBG dispersion compensation technique, for the launched laser power of 26dBm and link gain of 4dB, Q-factor value has degraded below the threshold of 6 after 500 spans with a total signal transmission of 12500km, where signal transmission distance has been raised significantly, as compared to Ref [6]. Higher results have been achieved using inline symmetrical and post-dispersion compensation, compensating inline and any nonlinear effects before entering the receiver. However, high transmission distance is severely affected, because the laser power is considered as high as 26 dBm, this has resulted in high optical nonlinear effects. For one channel system, third order distortion mechanism will generate TOH.

To multichannel system (WDM), distortion mechanism it will generate third order nonlinearity which will cause number of cross products such as four-way mixing (FWM), cross-phase modulation (XPM) and self-phase modulation (SPM) [27] and [28]. We have carried out similar investigations for various span lengths, achieving longer transmission distances, as illustrated in Fig. 15a.

- *At the laser power of 14dBm and gain of 16dB.*

By decreasing the launched laser power to 14dBm and amplifying the channel link with 16dBm, the Q-Factor value has degraded below the threshold of 6 after 520 spans, which in total is a signal transmission of 13000km, as shown in Fig.15b. However, from Fig. 15b

it is apparent that the Q-Factor hasn't changed significantly, as compared to previous example, shown in Fig. 15a. This concludes that by using the CS-SSB modulation for the same bandwidth, we can use half of the transmitted laser power. When comparing our proposed novel approach with the configuration published in existing literature Ref. [6, 17, 25], we have achieved a stable Q-Factor, high bitrate and a much longer signal transmission distance. With the use of proposed RoF optic communication architecture, we have extended the transmission distance up to 200km without any DC, as illustrated in Fig. 14b. The number of repeaters is minimised, and signal transmission distance has been raised significantly, as illustrated in Fig. 15 (a and b). This was achieved with only half of the power entering the modulator, as shown in Fig 15.b. With our proposed modulation format, the modulator has encoded 10Gbit/s of data at the pseudo-random binary sequence, compared to 2.5 Gbit/s encoded by Ref. [17].
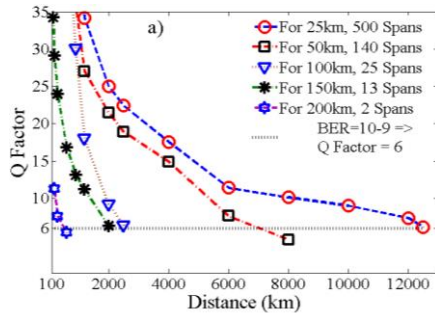

Fig. 15a. Q-Factor as a function of various signal transmission distance, using CS-SSB modulation SMF at 10Gbit/s Laser power of 26dBm, and gain power of 4dB.
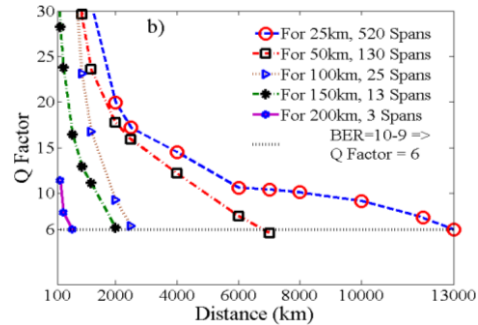
Fig. 15b. Q-Factor as a function of various signal transmission distance, using CS-SSB modulation, SMF at 10Gbit/s, Laser power of 14dBm, and gain power of 16dB

- *At the laser power of 4dBm and gain of 26dBm.*

For the launched laser power of 4dBm and link amplified with a gain of 26dB for various span lengths, the Q-Factor for the span length of 25km has degraded below the threshold of 6 after 350 spans, which is the total length of 8500km. Compared to previous input power, the signal transmission distance has decreased for 4500km, this is due to a decrease in the other half of the launched laser power, as illustrated in Fig. 15c. Compared to the conventional DC schemes, the signal transmission distance with linear FBG is raised noticeably. This originates from the high input power which can be used at liner FBG compensation. When using DC fibres, the signal decreases rapidly, as illustrated in Fig. 14a. This comes from DCF's low input power (intensity) handling capability, which results from the small effective area [26].
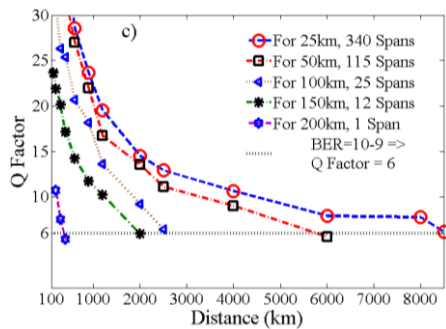

Fig. 15c. Q-Factor as a function of various signal transmission distance, using CS-SSB modulation, 10Gbit/s, Laser power of 4 dBm, and gain power of 26 dB
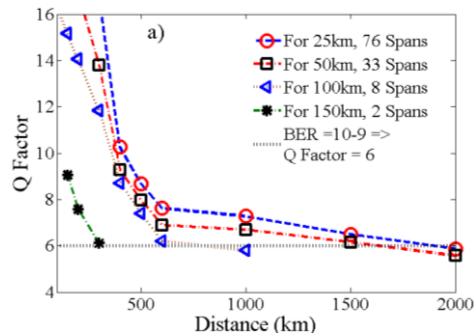
Fig. 16a. Q-Factor as a function of various signal transmission distance, using CS-SSB modulation, at 40Gbit/s, Laser power of 26 dBm, and gain power of 4 dB

For the Wave Division Multiplexing (WDM), nonlinear effects are a major problem, not only for power fading at the modulator but also for group velocity dispersion (GVD) and four-way mixing, causing crosstalk between the channels [27], [28].

By raising bitrate to 40 Gbit/s and comparing with the 10 Gbit/s, the transmitted signal distance degrades. For the launched laser power of 26dBm, and link gained with 4dB at the span length of 25 km, we have achieved a span ratio of 76, with a total link distance of 2000 km. This is far below the previous 10 Gbit/s signal transmission, as illustrated by Fig. 16a. Following on, we decrease the launched laser power to 14dBm and we amplify the channel link with 16dB for the span length of 25km. By using this setting, the number of achieved spans is 100, which is the signal transmission distance of 2500km and we have extended the transmission distance to 200km without any DC as shown in Fig.16b. This transmitted signal distance, at bitrate of 40 Gbit/s, is a higher signal transmission distance as compared to previous DC at bitrate of 10 Gbit/s reported in Ref. [1] and [6].

Fig. 16b. Q-Factor as a function of various signal transmission distance, using CS-SSB modulation, 40 Gbit/s, Laser power of 14 dBm, and gain power of 16 dB

Fig. 16c. Q-Factor as a function of various signal transmission distance, using CS-SSB modulation, 40 Gbit/s, Laser power of 4 dBm, and gain power of 26 dB
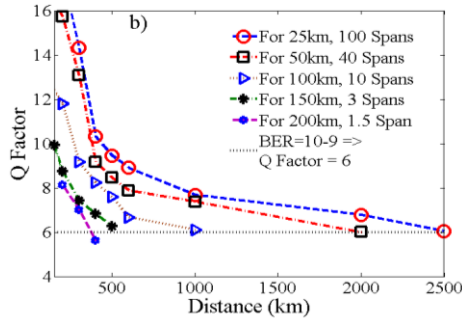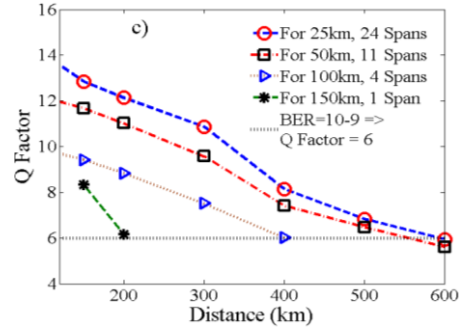
When observing all the generated data achieved from all the simulations, high transmission distance is severely affected by decreasing launched laser power to the minimum value and increasing link power to the maximum value. To achieve a Q-Factor higher than the threshold of 6, the link distance has decreased noticeably, and we could only achieve 24 spans for the span length of 25 km, which is the signal transmission distance of 600km, demonstrated in Fig.16c.

The main factors limiting the transmission distance and high bandwidth are nonlinear effects at the modulation and nonlinear optical properties presented in the fibre. At the high level of power, in one of the cases for the power of 26dBm, optical fibre shows these nonlinear properties as pulse speeding in the single mode fibre, and cross-talk between waves of different wavelengths in the WDM, caused as a factor of refractive index change and Amplified Spontaneous Emission (ASE).

These nonlinear effects will transfer energy from one channel to the other called FWM, and modulating itself or others called SFM and XPM respectively, by affecting the phase of the signal and causing spectral broadening. When the signal is transmitted it will cause GVD. GVD can accrue as induction of the pulse broadening, induction of the pulse chirping and the pulse compression [27, 28]. After a certain distance, it is necessary to amplify the link. The signal will be restored to an extent. However, by raising the input link power, all nonlinear effects such as Amplified Spontaneous Emission (ASE) noise will be amplified. Each time we amplify the link, optical signal to noise ratio degrades, and this is due to more ASE noise added to the system link [29, 30].

However, by the minimum transmission point applied to both modulators, we have achieved linearized optical SSB with suppressed carrier, which has increased the gain and effectiveness of the transmitted signal, planed Fig. 10, and Eq.29. When utilising proposed

CS-SSB we have suppressed nonlinear effects at the modulation, such as maximum suppression of TOH, cancelling SOH and achieving high SFDR of 50.48 [dBm] at the output of transmitter and high spurious suppression ratio of SFDR=49.58 dBm at the receiver side, as illustrated in Fig. 11. (a, b).

By considering the nonlinear effects at the modulation, and linear FBG dispersion compensation at the channel link, we can conclude that the transmission of higher bandwidth signals through a long-distance fibre optic system link is visibly raised, as compared to conventional DCF.

6. Conclusion

In this paper, we have developed and demonstrated a theoretical and simulation analysis of CS-SSB signal generation, using DP-DDMZM, in addition to signal transmission using two different loss compensators. The theoretically derived equations and simulation results are well matched, revealing that the CS-SSB modulation signal has resulted in high SFDR exceeding 50.48 dBm. We have demonstrated the CS-SSB modulation for the fibre link in long distance transmission, where we have extended the length of the link for the existing infrastructure, carried out and reported in Ref. [6, 17, 19], from 2400km to 13000km. By varying power between the laser and the link for the same bandwidth, we have demonstrated that we only require half of the transmitted laser power to achieve significant RoF system performance. For the bitrate of 10 Gbit/s and span length of 25 km, we have achieved a span ratio of 520 at the existing structure, compared to 2.5 Gbit/s encoded by Ref. [17], where we believe, configuration scheme is less complex and more cost-efficient. We have demonstrated that with the proposed CS-SSB modulation and appropriate map of linear compensation, we can reduce the effect generating the fibre dispersion, and enhance the optical spectral efficiency. The results show that our proposed RoF optic communication architecture can support up to 200km signal transmission for each span without any DC, while signal quality is kept stable during the transmission, as illustrated in Fig. 16b and simulated eye diagram, Fig.14b. The results obtained from this study will have a significant impact on reducing the reducing the cost (less repeaters), system's complexity, avoiding the usage of expensive devices over existing fibre at the long-reach and long-haul data transmission.

References:

[1] N. B. Pavlovic and A. V. T. Cartaxo, "Optimization of Single-Sideband DCS-RZ Format for Long-Haul 43-Gb/s/channel Ultradense WDM Systems," *Journal of Lightwave Technology*, vol. 25, no. 2, (2007) pp. 481-489

[2] Y. Cui, K. Xu, J. Dai, X. Sun, Y. Dai, Y. Ji, and J. Lin., "Overcoming Chromatic-Dispersion-Induced Power Fading in ROF Links Employing Parallel Modulators," *IEEE Photonics Technology Letters*, vol. 24, no.14, (2012) pp. 1173-1175.

[3] A. A. Fierra Junior, O. L. Coutinho, C. S. Martines, W. S. Fegadolli, H. A J. Ribeiro and J. E. B. Olivera, "Effect of Fibre Optic Chromatic dispersion on the performance of Analogue Optical Link with D.D Mach-Zehnder Modulator*" INTEL, ITA*, vil. 25, no 28 (2012).

[4] A. Ferreira, T. Silveira, D. Fonseca, R. Ribeiro and P. Monteiro, "Highly Linear Integrated Optical Transmitter for Subcarrier Multiplexed Systems," in *IEEE Photonics Technology Letters*, vol. 21, no.7, (2009) pp. 438-440.

[5] C. W. Chow, C. H. Yeh, Y. F. Liu, C. H. Wang, C. L. Wu and C. Chi, "Carrier Distributed PON Using SSB-CS Signal for Rayleigh Backscattering Suppression" *15th OECC, Sapporo Convention centre*, (2010).

[6] F. Paloi, T. Mirza, S. Haxha, "Optimisation of dispersion compensating in a long-haul fibre for RF transmission of up to 100 Gbit/s by using RZ and NRZ formats", Optik - International Journal for Light and Electron Optics, vol. 131, (2017) 640-654.

[7] A. Dar and J. Jha "Design and comparative performance analysis of different chirping profiles of tanh apodised fiber Bragg grating and comparison with the dispersion

compensation fiber for long-haul transmission system" *Journal Modern Optics*, vol. 64, no. 6, (2017), pp. 555-566.

[8] http://www.vpiphotonics.com/index.php

[9] C. Lim, A. Nirmalathas, K. L. Lee, D. Novak and R. Waterhouse, "Intermodulation Distortion Improvement for Fiber–Radio Applications Incorporating OSSB+C Modulation in an Optical Integrated-Access Environment," in *Journal of Lightwave Technology*, vol. 25, no. 6, (2007), pp.1602-1612.

[10] P. Devgan, A. Hastings, V. Urick, and K. Williams, "Cancellation of photodiode-induced second harmonic distortion using single side band modulation from a dual parallel Mach-Zehnder," Opt. Express vol. 20, (2012) pp. 27163-27173.

[11] X. Chen, W. Li and J. Yao, "Dynamic-Range Enhancement for a Microwave Photonic Link Based on a Polarization Modulator," in *IEEE Transactions on Microwave Theory and Techniques*, vol. 63, no. 7, (2015) 2384-2389.

[12] W. Freude, R. Schmogrow, B. Nebandahl, M. Winter, A. Jesten, S. Hillercus, J. Leuthold, "Quality metrics for optical signals: Eye diagram, Q-factor, OSNR, EVM and BER," *14th International Conference on Transparent Optical Networks*, Coventry, (2012), pp. 1-4.

[13] M. Xue, S. Pan and Y. Zhao, "Optical Single-Sideband Modulation Based on a Dual-Drive MZM and a 120° Hybrid Coupler," *Journal of Lightwave Technology*, vol. 32, no. 19, (2014), pp. 3317-3323.

[14] Z. Cao, J. Yu, L. Chen and Q. Shu, "Reversely Modulated Optical Single Sideband Scheme and Its Application in a 60-GHz Full Duplex ROF System," *IEEE Photonics Technology Letters*, vol. 24, no. 10, (2012), pp. 827-829.

[15] V. A. Thomas, M. El-Hajjar and L. Hanzo, "Millimeter-Wave Radio Over Fiber Optical Up-conversion Techniques Relying on Link Nonlinearity," IEEE *Communications Surveys & Tutorials*, vol. 18. No. 1, (2016), pp. 29-53.

[16] S. Shimotsu et al., "Single side-band modulation performance of a LiNbO3 integrated modulator consisting of four-phase modulator waveguides," in IEEE Photonics Technology Letters, vol. 13, no. 4, (2001), pp. 364-366.

[17] C. W. Chow, C. H. Wang, C. H. Yeh and S. Chi, "Analysis of the carrier-suppressed single sideband modulator used to mitigate Rayleigh backscattering in carrier - distribution PON", *OPTICS EXPRESS*, vol. 19, no 11, (2011).

[18] F. Aflatouni and H. Hashemi, "Wideband tunable laser phase noise reduction using single sideband modulation in an electro-optical feed-forward scheme," Opt. Lett. Vol. 37, no. 2, (2012), pp. 196-198.

[19] C. T. Lin, J. Chen, S. P. Dai, P. C. Peng and S. Chi, "Impact of Nonlinear Transfer Function and Imperfect Splitting Ratio of MZM on Optical Up-Conversion Employing Double Sideband with Carrier Suppression Modulation," *Journal of Lightwave Technology*, vol. 26, no. 15, (2008), pp. 2449-2459.

[20] G. Dattoli, A. Torre - S. Lorenzutta, "Theory of Multivariable Bessel functions and elliptic modular functions" *Le Matematiche*, vol. 53, no. 2, (1998), pp. 387-399.

[21] V. A. Thomas, M. El-Hajjar and L. Hanzo, "Millimeter-Wave Radio Over Fiber Optical Upconversion Techniques Relying on Link Nonlinearity," IEEE *Commun. Surveys & Tutorials*, vol.18, no. 1, (2016), pp. 29-53.

[22] Y. Ogiso, Y. Tsuchiya, S. Shinada, S. Nakajima, T. Kawanishi and H. Nakajima, "High Extinction-Ratio Integrated Mach–Zehnder Modulator with Active Y-Branch for Optical SSB Signal Generation," in *IEEE Photonics Technology Letters*, vol. 22, no. 12, (2010), pp. 941-943.

[23] S. Li, X. Zheng, H. Zhang and B. Zhou, "Highly Linear Radio-Over-Fiber System Incorporating a Single-Drive Dual-Parallel Mach–Zehnder Modulator," in *IEEE Photonics Technology Letters*, vol. 22, no. 24, (2010), pp. 1775-1777.

[24] N. I. Eappen, A. Sangeetha, "Analysis and performance comparison of inverse dispersion compensation technique for standard optical fibres," Computational Systems and Communications (ICCSC), *First International Conference*, (2014), pp. 364-369.

[25] W. Jiang, Q Tan, W. Qin, D. Liang, X. Li, H. Ma, Z. Zhu, "A Linearisation Analogue Photonic Link with high-order intermodulation distortion suppression based on Dual-Parallel Mach-Zehnder Modulator, IEEE photonics society, vol. 7, no. 3, (2015).

[26] H. Ademgil, S. Haxha, "Endlessly Single Mode Photonic Crystal Fibre with Improved Effective Mode Area", *Journal Optics Communications*, vol. 285, (2012), pp. 1514-1518.

[27] J. Kaur, N. Sharma, "Effects of Amplified Spontaneous Emission (ASE) on NRZ, RZ and CSRZ modulation formats in single channel light-wave system", ETNCC, *International Conference*, (2011), pp. 61-64.

[28] Y. A. Shpolyanskiy, S. A. Kozlov and V. G. Bespalov, "Stimulated Raman scattering and four waves mixing with self-phase and cross-phase modulation of intense fs laser pulses," *Quantum Electronics and Laser Science Conference,* Baltimore, USA, vol. 128, (1999).

[29] S. P. Singh and N. Singh, "Nonlinear effects in optical fibres: origin, management and applications", *PIER* vol. 73, (2007) pp. 249-275.

[30] W. E. Sabin, E. O. Schoenike, "Single Sideband Systems and Circuits" McGraw-Hill, Inc. New York, USA, (1987).